C.P. No. 615

C.P. No. 615

MINISTRY OF AVIATION

AERONAUTICAL RESEARCH COUNCIL

CURRENT PAPERS

Flow Field and Pressure Distribution Measurements on Blunt-Nosed Bodies at M = 6.8:

Parts I and II

by

W. K. Osborne and J. F. W. Crane

LONDON: HER MAJESTY'S STATIONERY OFFICE

1962

FIVE SHILLINGS NET

R 26062

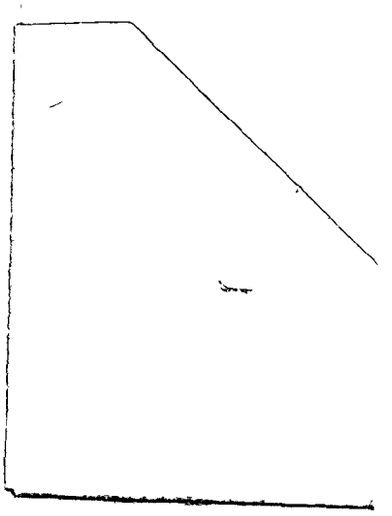

C.P. No.615

July, 1961

FLOW FIELD AND PRESSURE DISTRIBUTION MEASUREMENTS ON BLUNT-NOSED BODIES AT M = 6.8: PARTS I AND II

by

W. K. Osborne and J. F. W. Crane

SUMMARY

Part I describes the experimental measurement of sonic points between the bow shock waves and surfaces of three blunt-nosed bodies: a hemisphere, an ellipsoid and a hyperboloid. A comparison between these measurements and the theoretical sonic lines calculated by Mangler[1] shows reasonable agreement. Comparisons between the theoretical and the experimental bow shock wave shapes for these body configurations, together with their stand-off distances from the bodies, shows very close agreement.

Pressure distribution measurements along the surfaces of the ellipsoid and hyperboloid are described in Part II. On the forward part of the bodies a comparison between the experimental pressure distribution and the theoretical pressure distribution calculated by Mangler shows good agreement. However, agreement becomes progressively worse downstream. The experimental pressure distributions compare fairly well with the modified Newtonian pressure distributions for the two bodies. The location of the sonic points on the surfaces of the bodies, deduced from the experimental pressure distribution, gives values which are compatible with the sonic point measurements in Part I.

Previously issued as R.A.E. Technical Notes Nos. Aero 2707 and 2766. A.R.C. 22,372 and 23,437.

U.D.C. No. 533.6.011.72 : 533.696.7

FLOW FIELD AND PRESSURE DISTRIBUTION MEASUREMENTS ON BLUNT-NOSED BODIES AT M = 6.8

PART I

MEASUREMENT OF THE SONIC LINE, BOW SHOCK WAVE SHAPE AND STAND-OFF DISTANCE FOR BLUNT-NOSED BODIES AT M = 6.8

by

W. K. Osborne and J. F. W. Crane

LIST OF CONTENTS

LIST OF ILLUSTRATIONS

1 INTRODUCTION

In the flow field around a blunt-nosed body there is a subsonic region, near the stagnation point, between the bow shock wave and the body surface. The flow expands around the surface away from the stagnation point and eventually becomes supersonic. The locus of points, in a single plane, at which the flow attains sonic speed is known as the sonic line.

The interest and complexity of such a flow pattern, involving subsonic, transonic and supersonic regions has been such as to attract a large number of investigators. Two recent theoretical studies of this "supersonic blunt-body problem" are those of Mangler[1] and Van Dyke[2]. Mangler, for instance, has calculated the inviscid flow, including the sonic line, for axisymmetric bodies of various shapes at a free stream Mach number of seven.

An experimental check of this theoretical work is difficult because of the relative insensitivity of the more easily measured parameters, e.g. shock wave shape, stand-off distance and surface pressure in the subsonic region. A further measurement which can be made is of the location of the sonic line, employing an interfering-shock technique described by Kendall[3]: this may be more sensitive.

In proving the optical system of the R.A.E. 7 inch x 7 inch Hypersonic Tunnel, it was decided to check these features of the flow about three axisymmetric models whose contours spanned the range of shapes calculated by Mangler. In two cases (hyperbolic and elliptical nose shapes) there was good agreement between theory and experiment for shock wave shape, stand-off distance and location of the sonic line. For the hemisphere, good agreement was obtained for the shock wave shape and stand-off distance, but the location of the sonic line showed rather poorer agreement.

It is intended to extend these tests with pressure plotting models in the near future, and to measure pressure distributions well into the supersonic region.

2 DETAILS OF THE EXPERIMENTS

2.1 Description of models and probe

Fig.1 shows the three axisymmetric blunt nosed models which were designed to fit on the traverse sting in the hypersonic tunnel. The forward-facing surface of each model was of conic section, fitting the formula

$$y^2 = 2 R_B (x-x_{ST}) - B_B (x-x_{ST})^2 ,$$

where R is the nose radius and B the bluntness parameter. Suffix $( )_B$ refers to body surface parameters. (The suffix $( )_S$ is used later to refer to parameters for shock wave shapes, which are also known to be very nearly conic sections). x and y are rectangular coordinates, x being measured from the vertex of the bow shock wave and x_{ST} is the stand-off distance of the bow shock wave from the body.

The following parameters were chosen for the models in order that the results obtained could be compared with the results of Mangler's theoretical studies.

Model No.	B_B	R_B(ins)	Max. diam. of model (ins)
(1)	1·0	1·25	2·5
(2)	-0·671	0·5	3·0
(3)	2·0	2·0	2·83

The values of B_B are such that model (1) is circular, (2) is hyperbolic and (3) is elliptic in section.

A slender, pointed probe was designed to provide a weak shock wave to interfere with the bow shock wave and it was supported on a rod through the blank in the floor of the tunnel working section. Fig.2 shows how the probe was made adjustable by attaching the rod to a threaded support beneath the tunnel. The point of the probe was positioned several inches upstream of the model's leading surface.

2.2 Flow conditions

The free stream Mach number in the tunnel working section had a nominal value of 6·80, for all tests. However, there is a variation of ±1 per cent of this value across the stream tube containing the models[4].

2.3 Method of measurement and technique of testing

Direct shadow photography was used for recording full-size shock wave patterns on half plates mounted on the exit window. Exposure times (by flash tube) of two or three microseconds were used.

The model was set at zero incidence to the tunnel flow and the required position of the probe was set by the stop-nut. The probe was then temporarily retracted in order to minimize blockage during starting. All light was excluded from the working section and a photographic plate was loaded. The tunnel was started, the probe was returned to the selected position, and a shadowgraph picture was taken. The length of the runs was of the order of ten seconds.

2.4 Discussion of the sonic line tracing technique

The weak shock wave which is produced from the point of the probe is incident on the bow shock wave of the model and deflects as it is transmitted through. In the experiments the location of the point of the probe was adjusted so that the transmitted shock wave arrived in the sonic line region, after penetrating the supersonic region. In passing through the (low) supersonic region, the transmitted wave is gradually deflected and weak reflected waves build up into a reflected shock wave, as described by Robinson[5]. The transmitted and reflected waves meet at a cusp and this cusp is a sonic point. Thus by varying the probe position, a locus of sonic points is obtained, which is the sonic line.

Figs. 3(a), (b) and (c) are representative of photographs which show this pattern of transmitted and reflected waves meeting in a cusp. In others, the cusp was too near to the bow shock wave for the reflected wave to develop sufficiently to be seen: in such cases, the end point of the transmitted wave was taken to be the sonic point.

Each shadowgraph was analysed in the above manner by three independent observers and the mean values of their readings are plotted in Figs.4(a), (b) and (c). The individual readings varied by up to 6 per cent from these mean values.

3 PRESENTATION AND DISCUSSION OF RESULTS

In comparing the experimental results with the theoretical predictions, it should be remembered that the theory starts from a prescribed shape of bow shock wave and obtains a numerical solution for the resulting flow field, including a body shape. The experiments consisted of taking a set of such body shapes and determining the shock wave shapes and sonic points.

Figs.4(a), (b) and (c) show the shapes and locations of the shock waves and the measured sonic points in the flow for the three models tested and compare these with the theoretical results (including body shape). The numerical values of the various shock and body parameters are given in the inset tables. x and y coordinates are plotted non-dimensionally as a fraction of R_B, the body nose radius.

The graphs show good agreement between theory and experiment for bow shock wave and body surface shapes in the three cases. For the sonic line location reasonable agreement has been obtained in Figs.4(b) and (c) but agreement is not so good in Fig.4(a). (The theoretical sonic line in Fig.4(b) is indeterminate near the body).

Several factors must be taken into account to explain the considerable scatter of the experimental sonic points. Probably the most important factor contributing to the scatter is the difficulty in assessing the sonic point positions from the photographs. The point of reflection of the weak shock is not sufficiently well defined for accurate measurement, particularly when it is near to the bow shock wave or to the body surface. The definition is made more difficult by imperfections in the photographs due to marks on the tunnel windows. (As already mentioned individual readings varied by up to 6 per cent from the mean values plotted.)

One must also bear in mind the method of derivation of the theoretical flow field, i.e. from given bow shock wave shapes. The values of B_B for the resulting body shapes are fractionally different from the round numbers chosen for bodies (1) and (3) in the experiments. (The theoretical values are 0.964 as compared with 1.0 for model (1) and 1.991 as compared with 2.0 for model (3)). In addition, the theoretical results are calculated for a free stream Mach number of 7, while the Mach number in the tunnel working section was 6.8.

However, the above mentioned differences between the experimental and theoretical cases do not appreciably affect the shock wave and body shapes. In the former instance, this is because the differences between the theoretical and experimental values of B_B are sufficiently small to exclude serious changes in shape and in the latter instance, shock wave patterns in the region of investigation are practically frozen for $M \sim 5$. Figs.4(a), (b) and (c) compare the experimental shapes with check points of the theoretical shapes. Along the axis of the models the discrepancies are negligible and experimental bow shock wave stand-off distances agree with the corresponding theoretical values.

4 CONCLUSIONS

(a) Sonic line location

The results for the sonic lines are satisfactory considering the difficulties in assessing the experimental sonic points and fair agreement has been obtained between theory and experiment.

The experimental results are clustered near the centre of the region between the bow shock wave and the body surface. A refinement of the photographic technique would be desirable in future tests to enable points nearer the shock and the body to be obtained.

(b) Shock wave shapes and stand-off distances

The experimental bow shock wave shapes, and the stand-off distances, agree very closely with the theory, for all three cases.

In the near future it is intended to extend these results by carrying out tests on pressure plotting models having similar profiles to those used in the present tests.

LIST OF SYMBOLS

R_B Body nose radius

B_B Body bluntness parameter

R_S Bow shock wave nose radius

B_S Bow shock wave bluntness parameter

x, y Rectangular coordinates

x Coordinate measured downstream from the vertex of the bow shock wave

x_{ST} Stand-off distance of the bow shock wave from the body

---

LIST OF REFERENCES

Ref. No.	Author	Title, etc.
1	Mangler, K. W.	The calculation of the flow field between a blunt body and the bow wave. Colston Symposium, Bristol 1959. Hypersonic Flow - 1, Paper 10.
2	Van Dyke, M. D.	The supersonic blunt-body problem - review and extension. Journal of the Aero/Space Sciences, August, 1958.
3	Kendall, J. M.	Experiments on supersonic blunt-body flows. Progress report 20-372. California Institute of Technology, February, 1959.
4	Crane, J. F. W. Crabtree, L. F.	The 7 in. × 7 in. Hypersonic Wind Tunnel at R.A.E. Farnborough. A.R.C. C.P.590, August, 1961.
5	Robinson, A.	Wave reflection near a wall. Report No.37, College of Aeronautics, Cranfield. (A.R.C. 13,252) May, 1950.

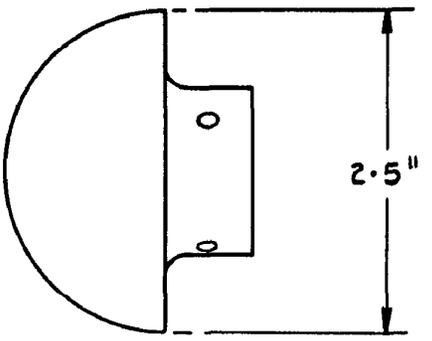

(a) MODEL (1) B_B = 1·0, R_B = 1·25 INS.

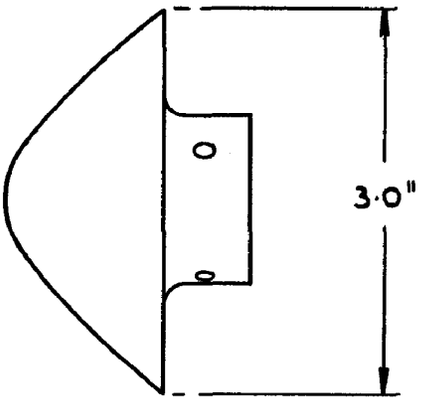

(b) MODEL (2) B_B = -0·671, R_B = 0·5 INS.

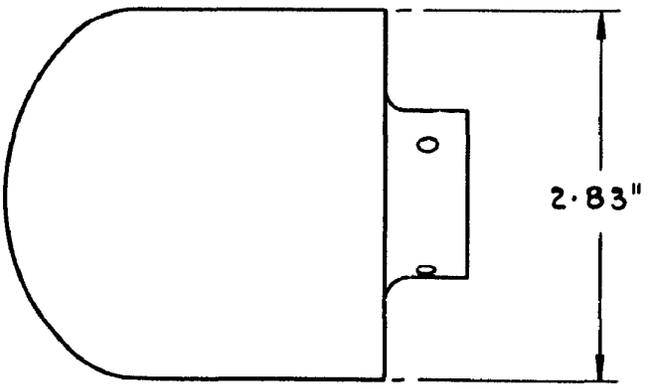

(c) MODEL (3) B_B = 2·0, R_B = 2·0 INS

FIG.1 DIAGRAMS OF MODELS TESTED

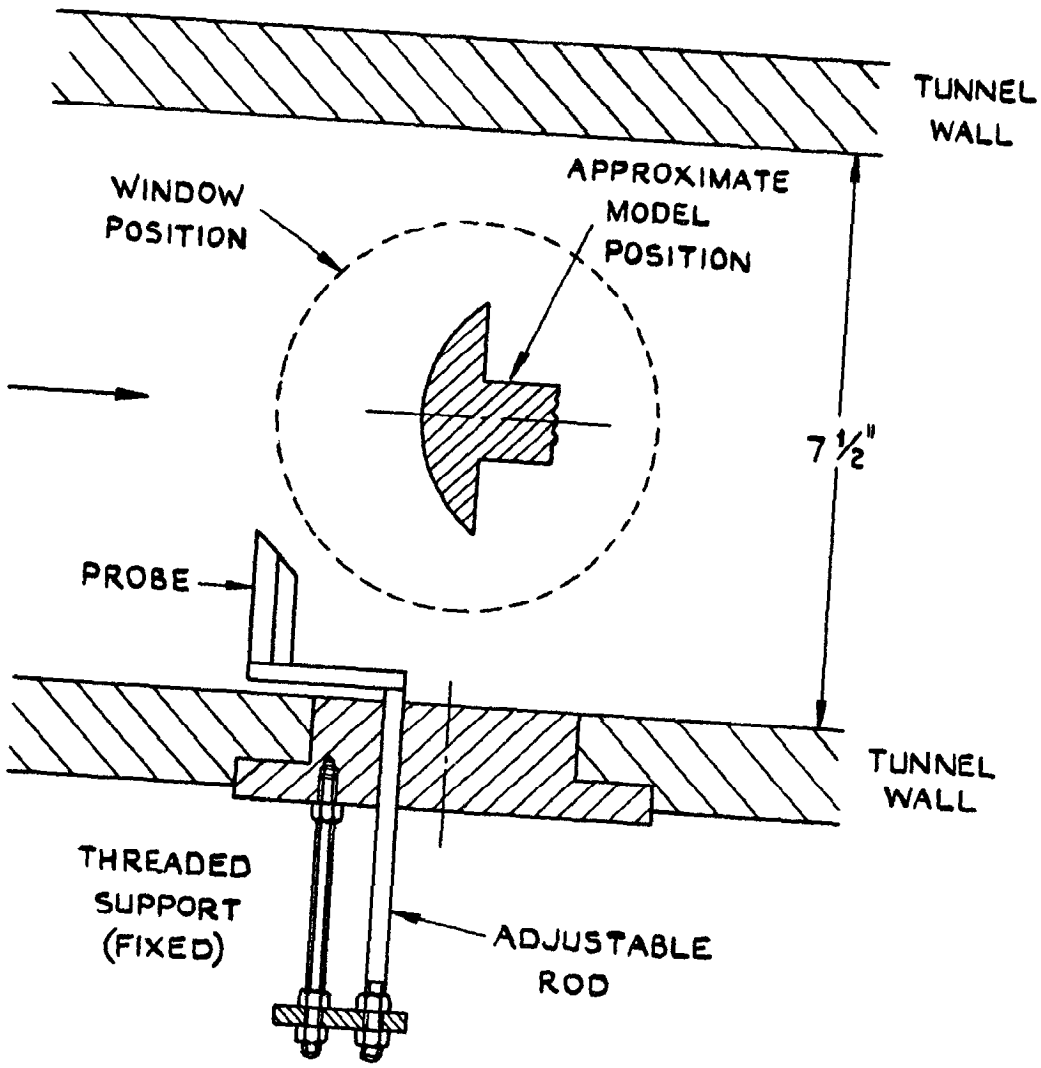

FIG. 2. DIAGRAM OF TEST APPARATUS
(TO SCALE)

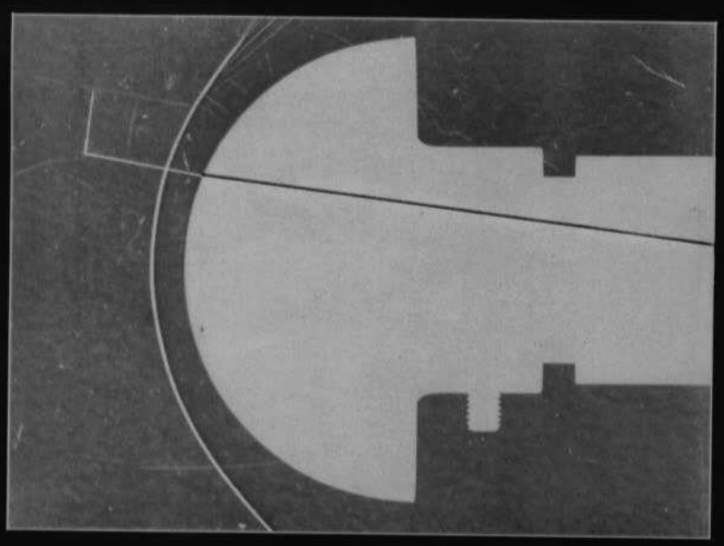

MODEL (1)
HEMISPHERE

INTERFERING SHOCK WAVE

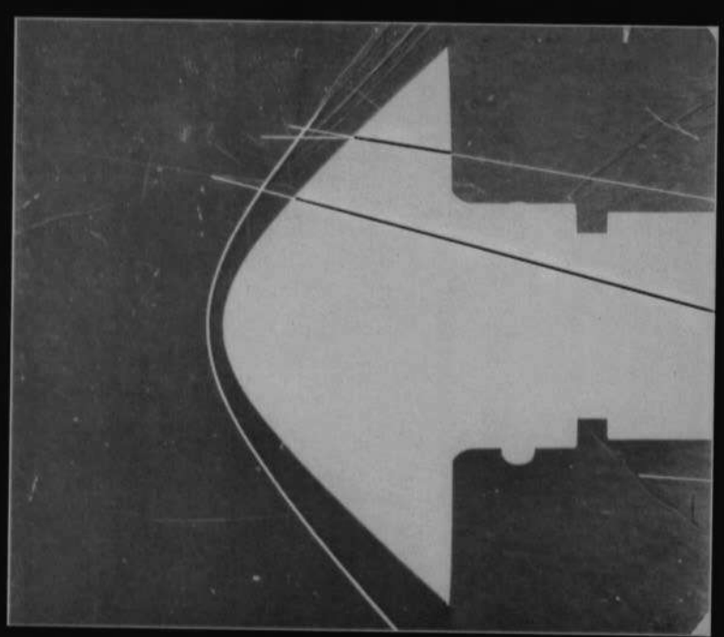

MODEL (2)
HYPERBOLIC SECTION

SCRATCHES ON WINDOWS

INTERFERING SHOCK WAVE

DISTURBANCE IN BOUNDARY LAYER ON WINDOW, CAUSED BY SHOCK WAVE FROM MODEL

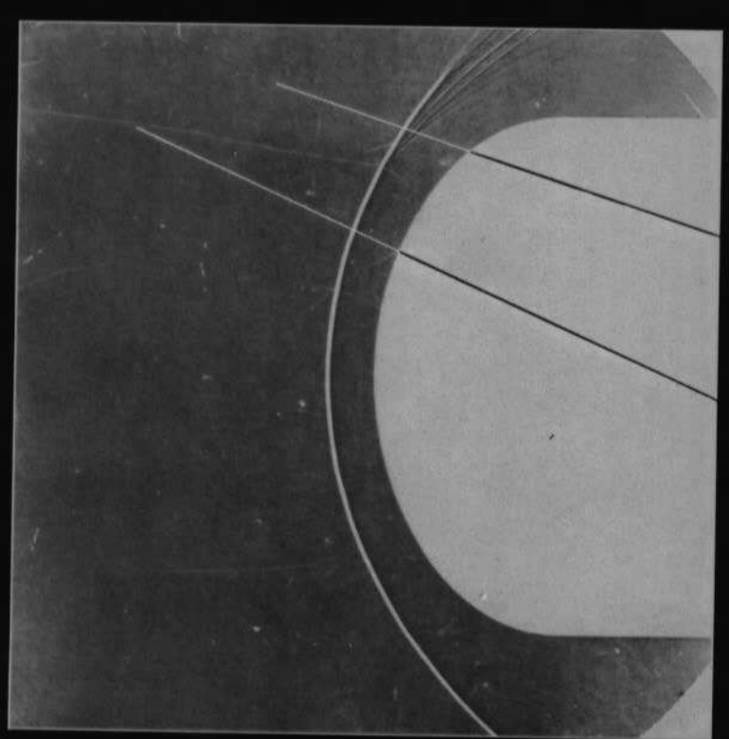

MODEL (3)
ELLIPTIC SECTION

WAKE FROM PROBE

INTERFERING SHOCK WAVE

FIG. 3. REPRESENTATIVE FLOW PICTURES SHOWING THE INTERFERING SHOCK WAVE METHOD FOR INDICATING THE SONIC LINE

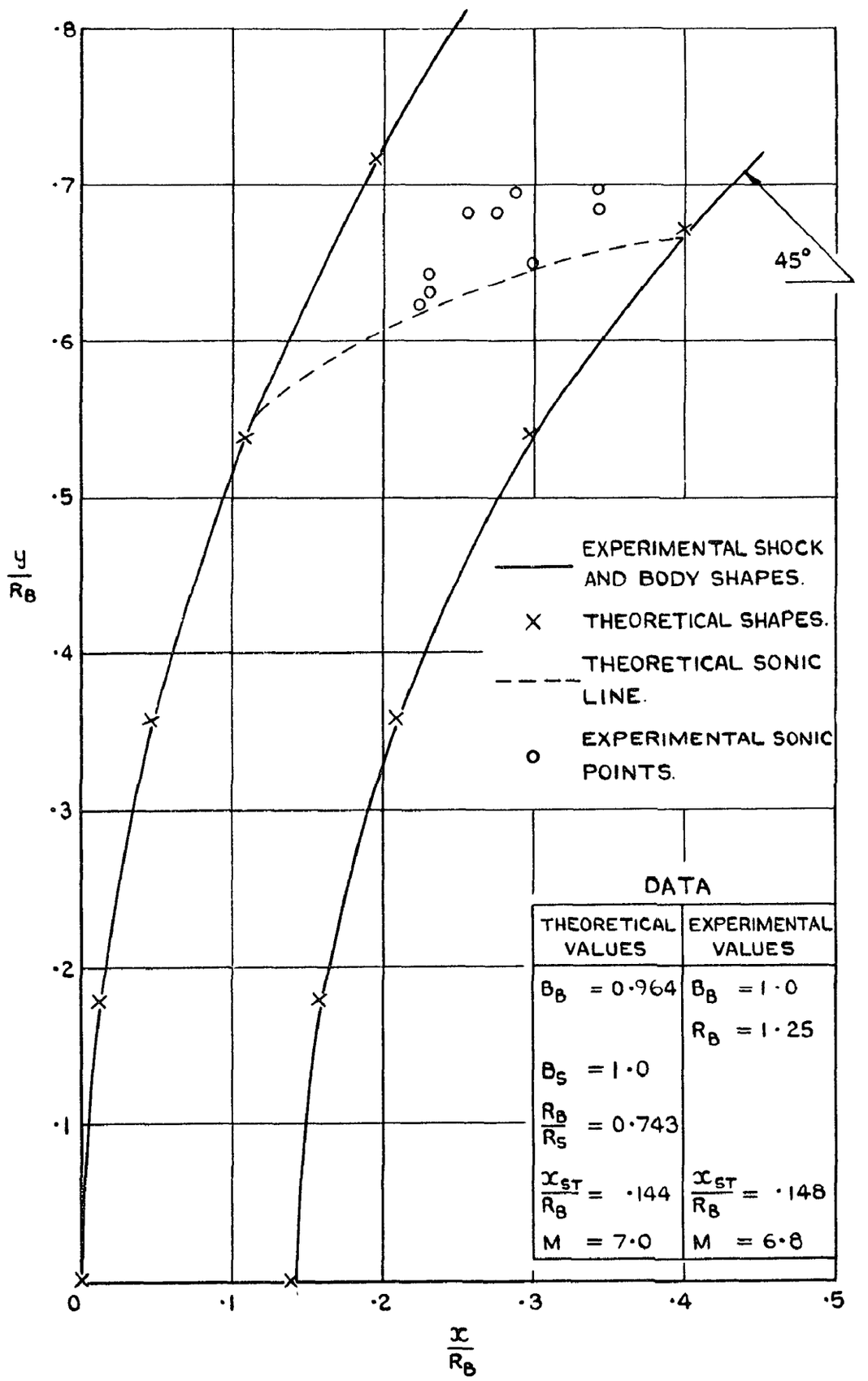

FIG. 4(a). MODEL (I); HEMISPHERE. COMPARISON OF MEASURED VALUES WITH THEORETICAL ESTIMATES.

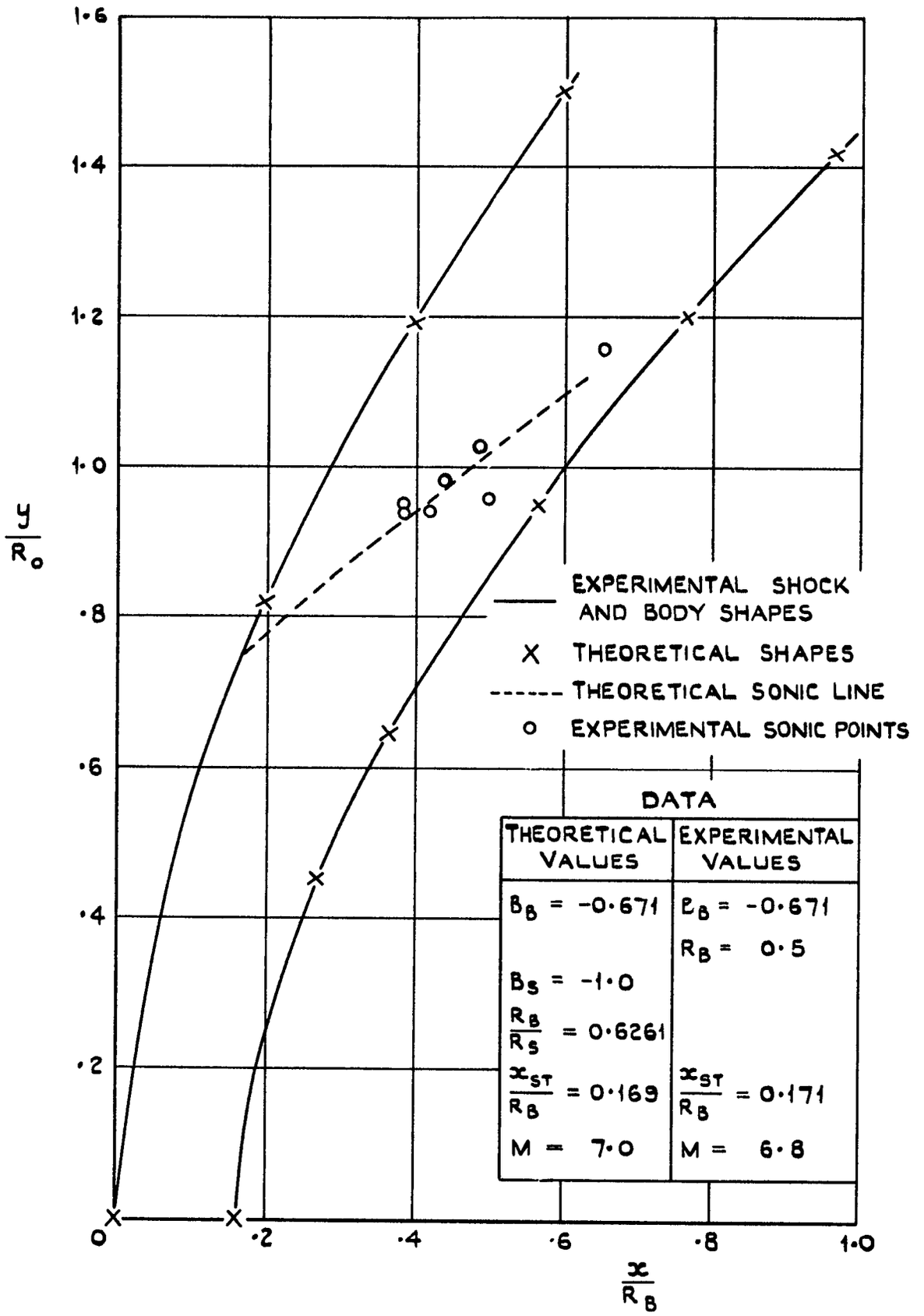

FIG.4(b). MODEL(2).COMPARISON OF MEASURED VALUES WITH THEORETICAL ESTIMATES.

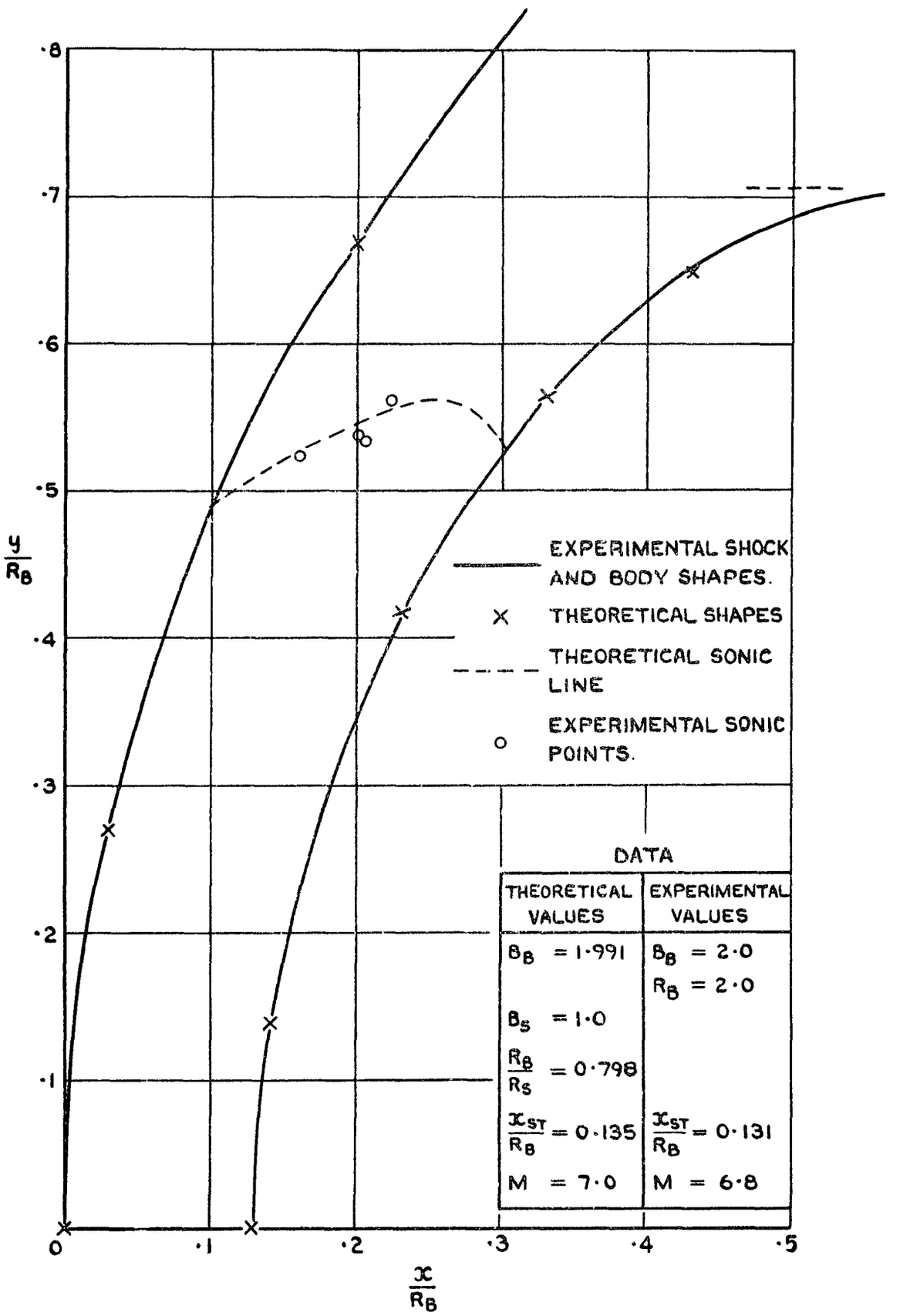

FIG. 4(c). MODEL (3). COMPARISON OF MEASURED VALUES WITH THEORETICAL ESTIMATES.

U.D.C. No. 533.696.7 : 533.6.048.2 : 533.6.011.55

FLOW FIELD AND PRESSURE DISTRIBUTION MEASUREMENTS ON BLUNT-NOSED BODIES AT M = 6.8

PART II

PRESSURE MEASUREMENTS ON TWO BLUNT-NOSED BODIES AT M = 6.8

by

W. K. Osborne

LIST OF CONTENTS

LIST OF ILLUSTRATIONS

1 INTRODUCTION

The flow field around a blunt-nosed body has been widely investigated, both theoretically and experimentally. Theoretical studies by Mangler[1] and Van Dyke[2], for example, have calculated the flow fields between the bow shock waves and the surfaces of axisymmetric blunt shapes. The method of Mangler starts from a prescribed bow shock wave shape and uses a marching technique to determine the inviscid flow field including the body shape which produces the prescribed shock. The flow fields about three axisymmetric blunt body shapes (hemisphere, hyperboloid and ellipsoid) which have been treated by this method were investigated in a recent experiment[3]. Bow shock wave shapes and stand-off distances were measured and the sonic line positions located, at a free-stream Mach number of 6.8. Good agreement was obtained between the results from theory and experiment for the shock wave shapes and stand-off distances. Comparison between the theoretical and experimental positions of the sonic line was limited (by the experimental technique) to the middle of the region between the bow shock wave and the surface of the body.

The sonic point on the shock wave is easily located from measurements of the shock angle, but the sonic point on the body must be obtained from a measured pressure distribution. Thus, the purpose of the present experiment (again designed for the 7 in. × 7 in. hypersonic tunnel running at $M = 6.8$) was to measure the surface pressure distribution on the hyperbolic and elliptic shapes. (The pressure distribution on a hemisphere has been reported elsewhere[4]).

The results have been compared with those from the theory and with the previous experimental results. The pressure distribution has also been compared with a modified Newtonian pressure distribution.

2 DETAILS OF EXPERIMENTS

2.1 Description of models and pressure measuring apparatus

Fig.1 shows the cross sections of the two axisymmetric blunt-nosed models which were used for the pressure measurements. The forward-facing surface of each model was of conic section fitting the formula

$$y^2 = 2R_B(x - x_{ST}) - B_B(x - x_{ST})^2,$$

where R is the nose radius and B the bluntness parameter. Suffix $(\ )_B$ refers to body surface parameters (the suffix $(\ )_s$ is used later to refer to parameters for bow shock wave shapes, which are also known to be very nearly conic sections). x and y are rectangular co-ordinates, x being measured from the vertex of the bow shock wave and x_{ST} is the stand-off distance of the bow shock wave from the body.

The parameters pertaining to the two models are as follows:

Model No.	B_B	R_B (in.)	Max. diameter of model (in.)
(1)	-0.671	0.5	2.99
(2)	2.0	2.0	2.83

The values of B_B are such that model (1) is hyperbolic and (2) is elliptic in section. These values were chosen so that a direct comparison could be made with the theoretical results of Mangler[1].

The models were stainless steel shells, 1/10 inch thick having a common backing plate which was designed to fit onto the hypersonic tunnel traverse sting. Hypodermic tubing, $1\frac{1}{2}$ mm outer diameter and 1 mm inner diameter was used to instrument the models with pressure holes. A hole diameter of 1 mm leads to a positive error[6] of about 1% in measuring surface pressures on these models, except for the cylindrical portion of model (2), where a positive error of nearly 10% is incurred. However, the pressures here are much lower than on the forward part of the model. The tubes were brazed so that they were flush with the model surface. Each model had a polished finish of better than 10 microns. Fig.1 shows the position of the pressure holes along a generator on each model. Model (1) was instrumented with 6 holes (hole number 6 was diametrically opposite to number 5 in order to check that the model was at zero incidence. Unfortunately, tubes 5 and 6 were damaged during the early tests and so only the results obtained from tubes 1 to 4 are quoted. However the zero incidence check was satisfactory. Model (2) was instrumented with 8 holes 4 of which were on a cylindrical after-body. The pressure tubing passed through the hollow traverse sting to the sting support and then outside the tunnel to a mercury manometer bank. The bank had seven vertical glass tubes with a common reservoir, and a clamp to isolate the bank from the model. To obtain a reference pressure for the manometer bank, one of the pressure holes was connected to a Midwood pressure balance in parallel with one of the manometer tubes.

2.2 Flow conditions

The free stream Mach number in the tunnel working section had a nominal value of 6.80 for all tests. However, there is a variation of ±1 per cent of this value across the stream tube containing the models[5]. The tunnel stagnation pressure was controlled at 750 p.s.i. (gauge), and the stagnation temperature was 680°K.

2.3 Method of pressure measurement

The model, at zero incidence to the tunnel flow, was positioned in line with the upstream windows, on the centre line of the tunnel working section. The pressure holes (with the exception of number 6 on model (1)) lay along the top generator. Pressure tubes from the model were connected to the manometer bank. Pressure hole number 1 (the stagnation point on both models) was connected to one of the manometer bank tubes in parallel with the Midwood pressure balance. The manometer bank clamp was closed before starting the tunnel so as to prevent the large (steady state) pressure differences between the tubes being magnified during the passage of the starting shock. This would have caused a mercury overflow in the tubes. When the flow had been established the clamp was released. The flow was continued until all the mercury columns and the Midwood pressure reading had reached steady values. The clamp was then closed and the tunnel was shut down. Readings were taken of the mercury levels and of the Midwood pressure balance. The tunnel stagnation pressure was also noted during the test.

Then, the model was inverted so that the pressure holes lay along the bottom generator. Several tests in each position were made until the readings repeated satisfactorily. Tunnel running time was approximately $\frac{1}{2}$ minute for each test.

3 PRESENTATION OF RESULTS

3.1 Theoretical values

The theory of Mangler assumes a prescribed bow shock wave shape and obtains a numerical solution for the resulting flow field including body shape. A numerical evaluation of the flow field at a free-stream Mach number, M_∞, of 7 is available, including the surface pressure distribution p/p_o for the two configurations under investigation (p is the surface static pressure and p_o is the pressure at the stagnation point). The values of p/p_o on the body surface can be converted to pressure coefficient form since

$$C_p = (p - p_\infty)/\tfrac{1}{2} \rho_\infty U_\infty^2 = (2/\gamma M_\infty^2)(p/p_o \times p_o/p_\infty - 1)$$

where p_∞, ρ_∞ and U_∞ are the free-stream static pressure, density and velocity respectively.

At $M_\infty = 7$, $p_o/p_\infty = 63.55$; hence C_p is obtained. Figs.2 and 3 show the theoretical value of $C_p/C_{p_{max}}$ obtained by Mangler plotted against the non-dimensional distance along the body surface, S/R_B, where S is measured from the stagnation point.

An alternative approximation to the flow over the forward part of blunt bodies is given by the modified Newtonian impact theory where

$$C_p = C_{p_{max}} \sin^2 \theta .$$

θ is the angle of inclination of the body surface to the free-stream flow direction. For model (1), where $R_B = 0.5$ in., $B_B = -0.671$, the equation of the profile is

$$Y^2 = X + 0.671 X^2$$

where X and Y are rectangular co-ordinates with the origin at the body vertex. This gives

$$C_p/C_{p_{max}} = \sin^2 \theta = (1 + 2.684X + 1.801X^2)/(1 + 6.684X + 4.485X^2).$$

For model(2), where $R_B = 2.0$ in. and $B_B = 2.0$, the equation of the profile is

$$Y^2 = 4X - 2X^2,$$

which gives

$$C_p/C_{p_{max}} = \sin^2\theta = (2X^2 - 4X + 2)/(X^2 - 2X + 2).$$

Stations X are related to S; thus the modified Newtonian values of $C_p/C_{p_{max}}$ may be plotted and are shown in Figs.2 and 3.

3.2 Experimental values

The pressure coefficient may be calculated from the values of p obtained on the manometer, since

$$C_p = (p - p_\infty)/q, \qquad \text{where } q = \tfrac{1}{2}\rho_\infty U_\infty^2 .$$

At $M_\infty = 6.8$, $p_\infty = 0.2902 \times 10^{-3} \times P_o$ (p.s.i. abs.) and $q = 0.9395 \times 10^{-2} \times P_o$ (p.s.i. abs.). Figs.2 and 3 show the experimental values of $C_p/C_{p_{max}}$ on the model surface.

The position of the sonic point is determined by

$$p/p_o = \left[1 + \{(\gamma-1)/2\} M^2\right]^{\frac{\gamma}{1-\gamma}}$$

whence at M = 1, on the model surface,

$$p/p_o = 0.5283 \quad \text{for } \gamma = 1.4$$

and

$$C_p/C_{p_{max}} = 0.521.$$

Figs.2 and 3 show the sonic point positions on the two models measured along S. In Figs. 4 and 5, the sonic line locations of a previous experiment[3] are shown, and the present locations of the sonic points on the model surfaces are added.

3.3 Discussion of results

Comparison of the experimental and the theoretical pressure distributions obtained by Mangler in Figs.2 and 3 shows close agreement near the forward part of the models but agreement becomes gradually worse downstream. For model (1) the percentage difference in $C_p/C_{p_{max}}$ referred to the experimental value at $S/R_B = 1.6$ is 5; thereafter increasing rapidly. For model (2) the curves cross at $S/R_B = 0.68$. When $S/R_B < 0.68$ the percentage difference in $C_p/C_{p_{max}}$ reaches a maximum of 7 and for $S/R_B > 0.68$ the difference increases continuously.

The experimental sonic point on the surface of model (1) is at $S/R_B = 1.98$ which is compatible with the experimental sonic line location shown in Fig.4. The theoretical calculations of the sonic line location (and surface pressure distribution) for body No.1 have been extended to larger values of S since the publication of Ref.3. It turns out that for this particular body the inviscid flow near the surface never reaches sonic velocity. That a sonic point on the body was obtained in the experiments is probably due to the fact that the calculations assume an infinite body but the model of Fig.1(a) was cut off at a value of S = 1.98 inches. It would be interesting to test models which extend to larger values of S in order to check whether the sonic point moves back along the surface.

On model (2) the experimental and theoretical positions of the sonic point on the surface are in fairly close proximity, as shown in Figs.3 and 5.

During repeated tests on each model the values of C_p showed a deviation of less than one per cent from the mean of values measured at a given station, except for very low values of C_p (0.04 on the cylindrical section of Model (2) where deviations of up to 5 per cent occurred.

Discrepancies between theory and experiment in the sonic point region (in addition to the difference between theoretical and experimental models of body No.1 mentioned above) may be due also to the computer programme, devised to enumerate the flow field between the bow shock wave and surface of these blunt bodies. The nature of the programme was such as to cause increasing inaccuracy downstream. This is being investigated further.

The modified Newtonian pressure distribution underestimates the experimental values on model (1) over the whole surface and overestimates them on model (2) from the stagnation point almost up to the junction of the ellipsoid and cylinder, where the Newtonian value of $C_p/C_{p_{max}}$ falls to zero.

4 CONCLUSIONS

The pressure distributions on a hyperboloid and on an ellipsoid have been measured, and the results compared with those from the theoretical studies of Mangler[1]. Good agreement was obtained on the forward part of the models. Near the sonic point region rather poorer agreement was obtained for the hyperboloid. For the ellipsoid fair agreement was obtained in this region but agreement became poor near the junction of the ellipsoid and cylinder.

The location of the sonic points on the two models was shown to be consistent with previous experiments. In the case of the ellipsoid the experimental determination of the sonic point position was close to the theoretical estimate.

A comparison of the experimental with the modified Newtonian pressure distribution showed fair agreement.

LIST OF SYMBOLS

R_B	body nose radius
B_B	body bluntness parameter
R_S	bow shock wave nose radius
B_S	bow shock wave bluntness parameter
x,y	rectangular co-ordinates with x measured downstream from the vertex of the bow shock wave
x_{ST}	stand-off distance of the bow shock wave from the body
X,Y	rectangular co-ordinates with X measured downstream from the vertex of the body
p	static pressure on the body surface
p_o	stagnation point pressure
P_o	free stream total pressure
p_∞	free stream static pressure
ρ_∞	free stream density
U_∞	free stream velocity
M_∞	free stream Mach number
S	distance along body surface from stagnation point
θ	angle of inclination of body surface to the free stream flow direction

---

LIST OF REFERENCES

No.	Author	Title, etc.
1	Mangler, K. W.	The calculation of the flow field between a blunt body and the bow wave. Proceedings of the Hypersonics Colston Symposium, Bristol, 1959. Published by Butterworths Scientific Publications, 1960.
2	Van Dyke, M. D.	The supersonic blunt body problem - review and extension. Journal Aero/Space Sciences, 25, pp.485-494. August, 1958.
3	Osborne, W. K. Crane, J. F. W.	Measurement of the sonic line, bow shock wave shape and stand-off distance for blunt-nosed bodies at M = 6.8. Part I of this Current Paper.

LIST OF REFERENCES (CONTD.)

No.	Author	Title, etc.
4	Crawford, D. H. McCauley, W. D.	Investigation of the laminar aerodynamic heat-transfer characteristics of a hemisphere-cylinder in the Langley 11 inch hypersonic tunnel at a Mach number of 6.8. N.A.C.A. Report 1323 1957.
5	Crane, J. F. W.	The 7 in. × 7 in. hypersonic tunnel at R.A.E. Farnborough. Part III. Calibration of flow in the working section. A.R.C. C.P.590. August, 1961.
6	Rayle, R. E. Jr.	Influence of orifice geometry on static pressure measurements. A.S.M.E. Paper No. 59-A-234. (1959).

WT.2078.C.P.615.K3 - Printed in England

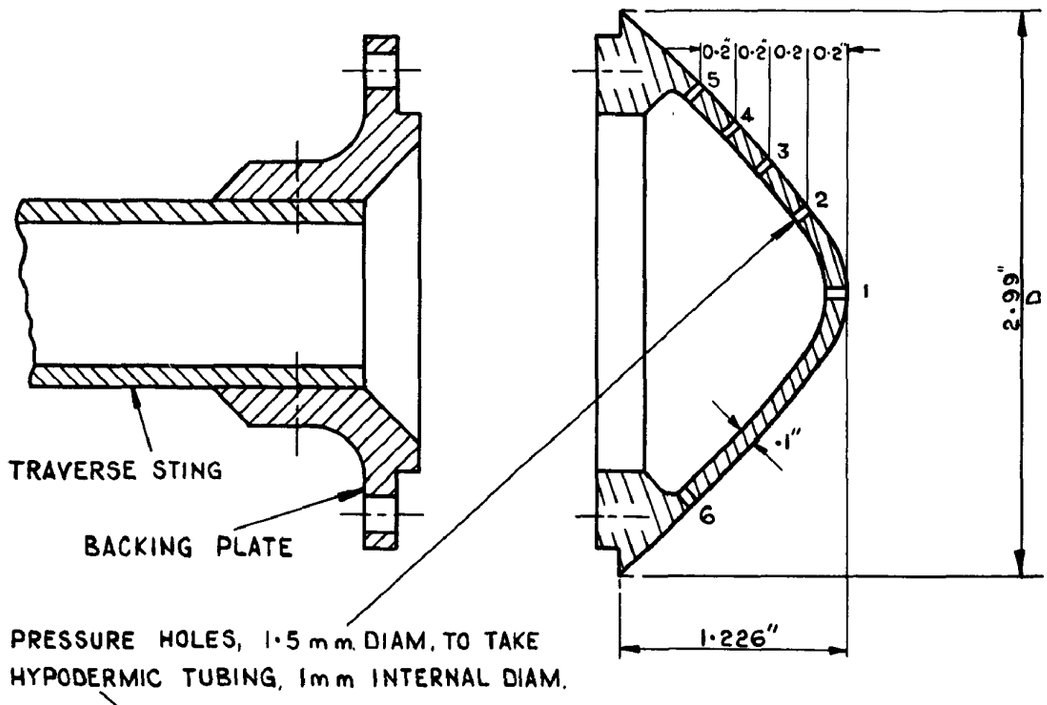

(a) MODEL (1), R_B = 0·5 INS., B_B = −0·671

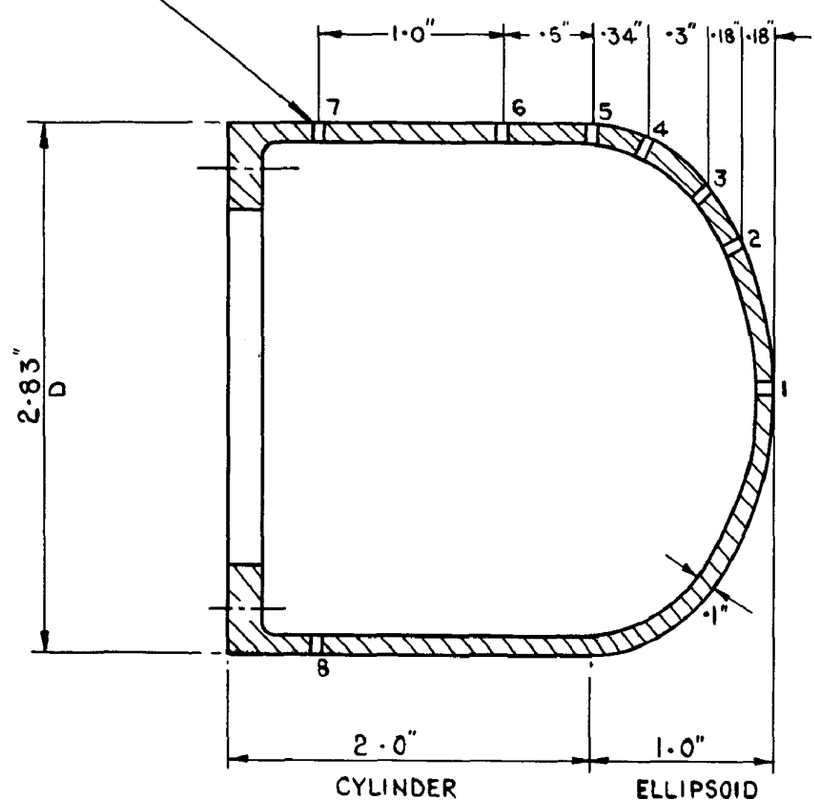

(b) MODEL (2), R_B = 2·0 INS., B_B = 2·0

FIG. 1 CROSS SECTIONS OF PRESSURE PLOTTING MODELS.

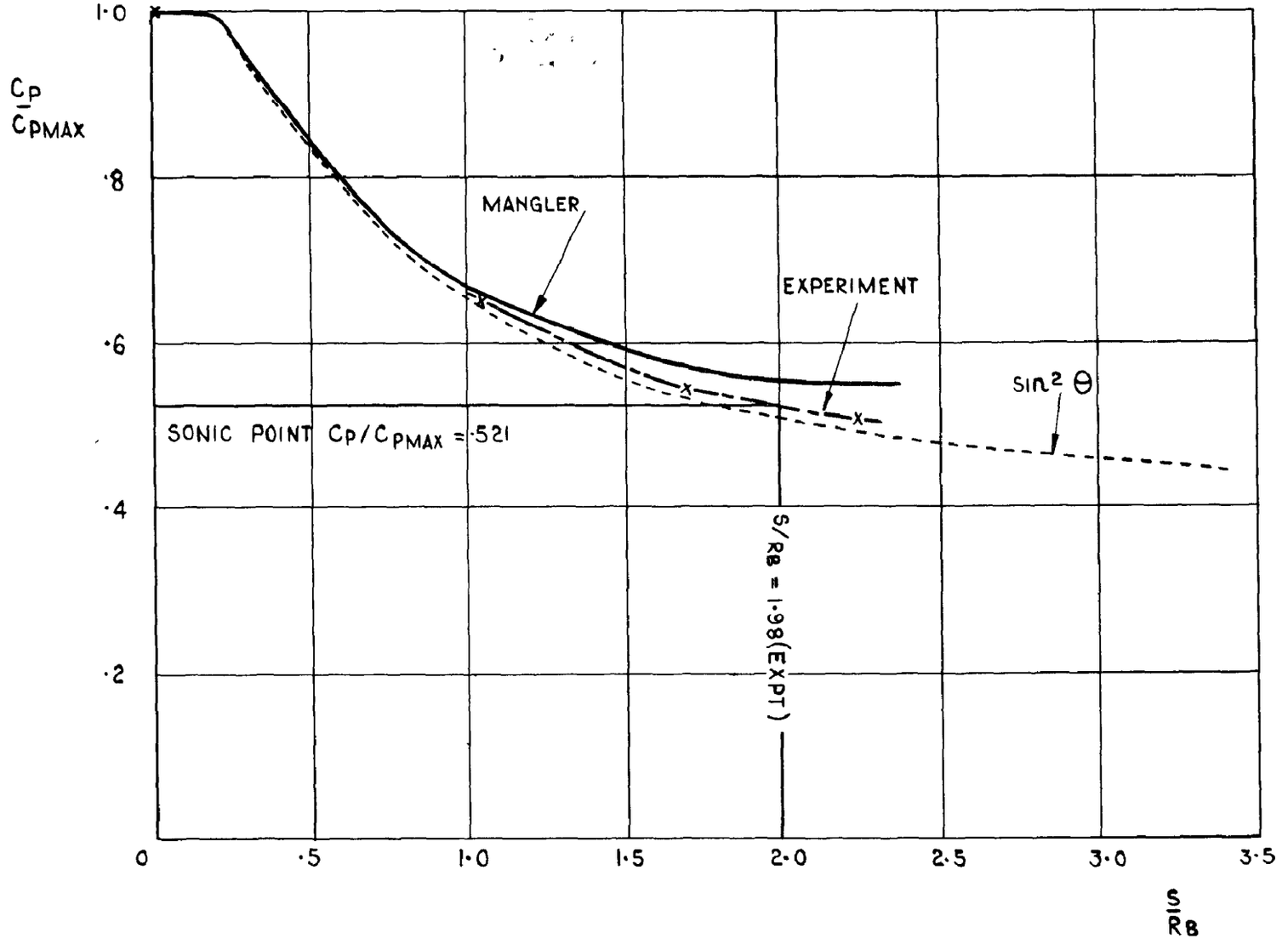

FIG. 2 PRESSURE DISTRIBUTION ON MODEL (1).

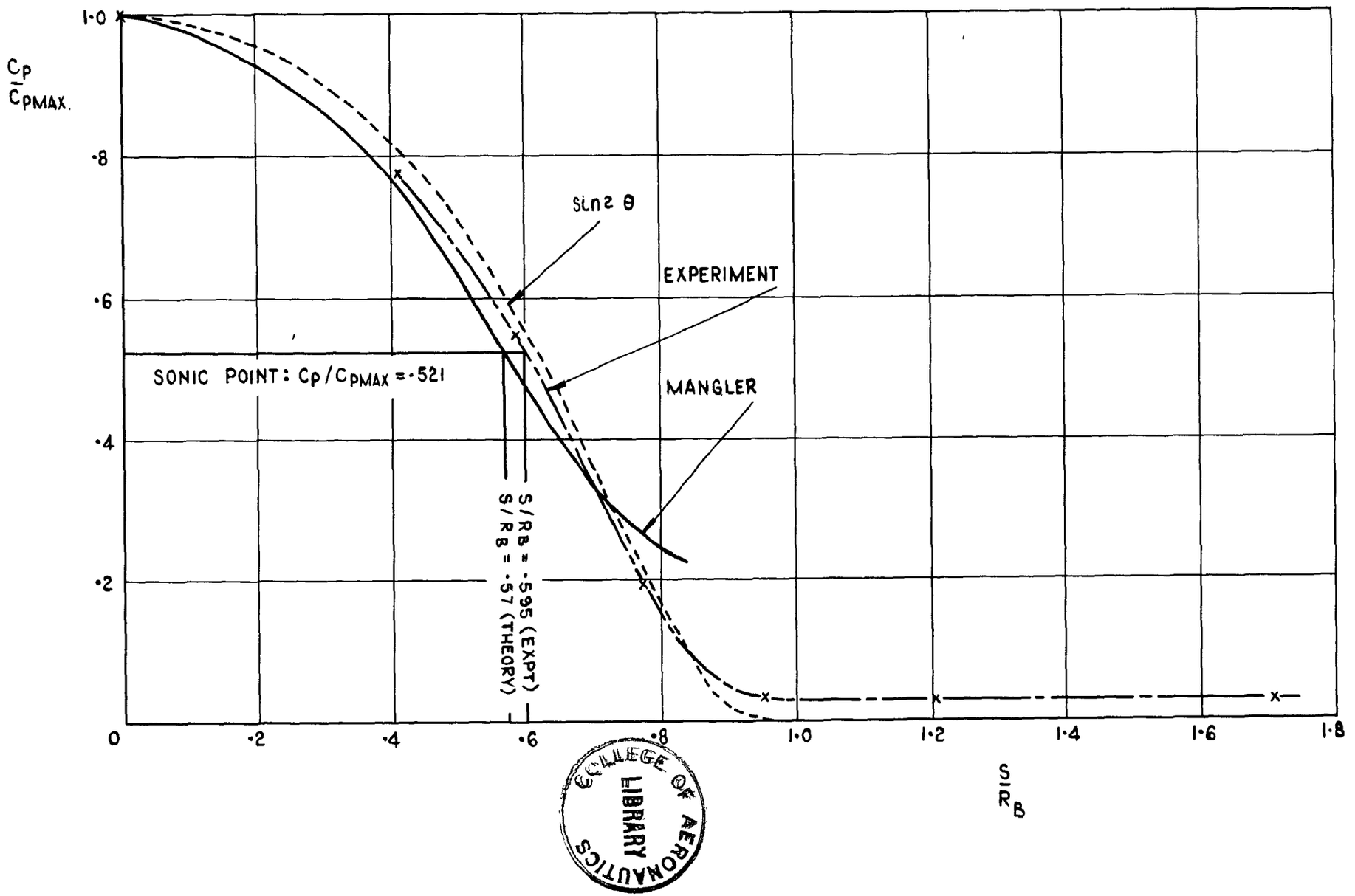

FIG. 3 PRESSURE DISTRIBUTION ON MODEL (2).

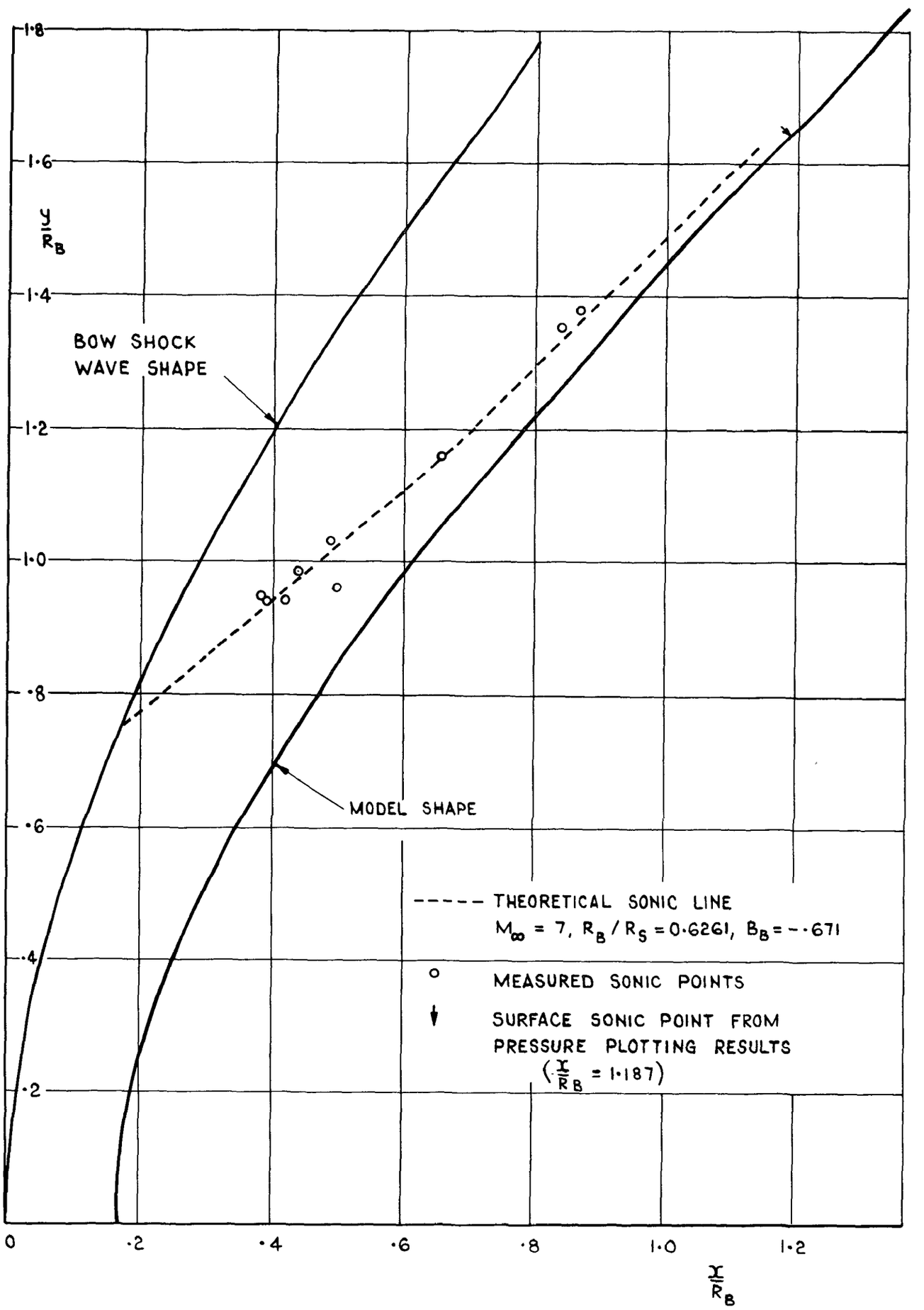

FIG.4 SONIC POINTS FOR MODEL (1); HYPERBOLOID.

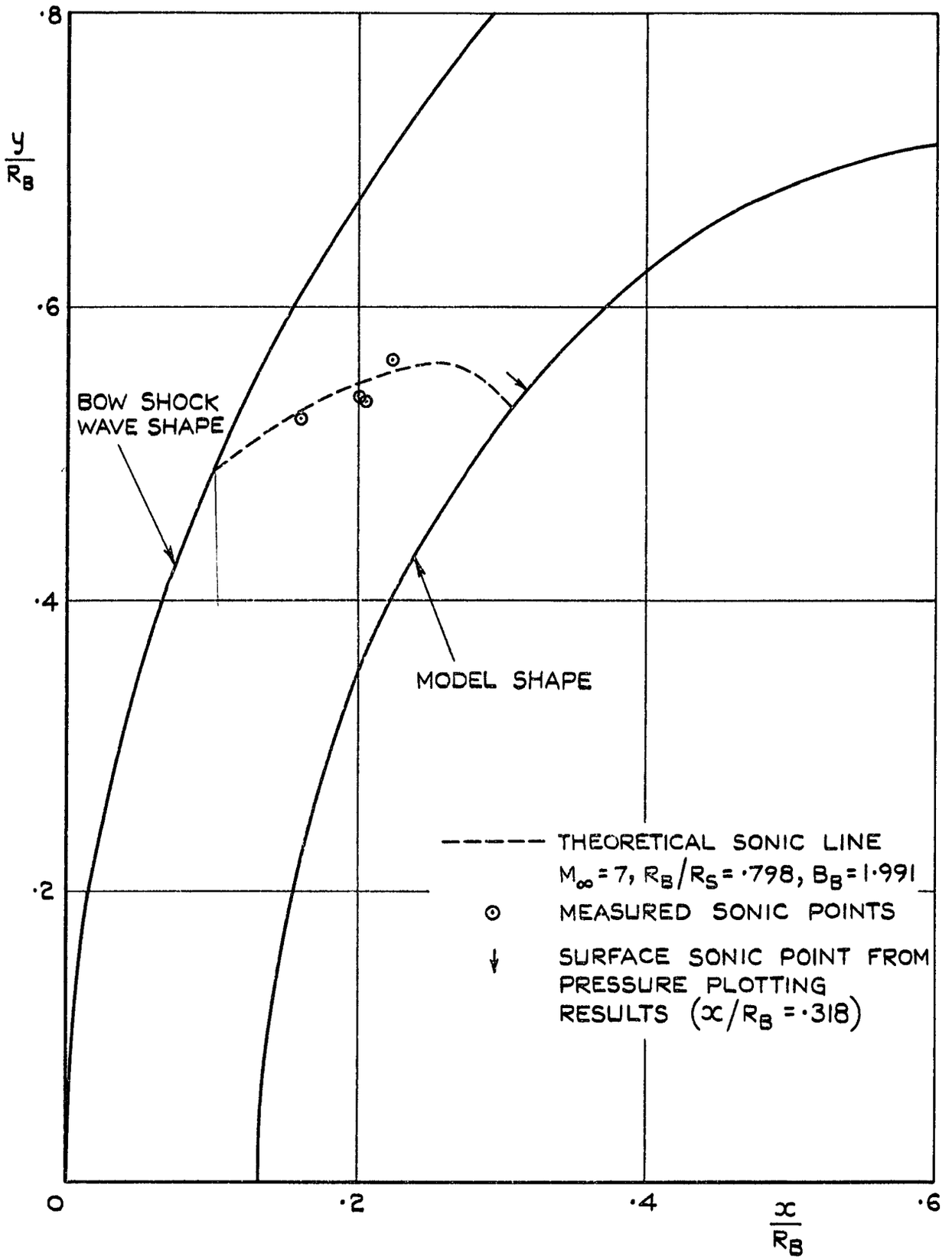

FIG. 5. SONIC POINTS FOR MODEL (2); ELLIPSOID.

A.R.C. C.P. No.615. July, 1961
Osborne, W.K. and Crane, J.F.W.

FLOW FIELD AND PRESSURE DISTRIBUTION MEASUREMENTS ON BLUNT-NOSED BODIES AT M = 6.8. PARTS I AND II.

Part I describes the experimental measurement of sonic points between the bow shock waves and surfaces of three blunt-nosed bodies: a hemisphere, an ellipsoid and a hyperboloid. A comparison between these measurements and the theoretical sonic lines calculated by Mangler[1] shows reasonable agreement. Comparisons between the theoretical and the experimental bow shock wave shapes for these body configurations, together with their stand-off distances from the bodies, shows very close agreement.

Pressure distribution measurements along the surfaces of the ellipsoid and hyperboloid are described in Part II. On the forward part of the bodies a comparison between the experimental pressure distribution and the theoretical pressure distribution calculated by Mangler shows good

(Over)

A.R.C. C.P. No.615. July, 1961
Osborne, W.K. and Crane, J.F.W.

FLOW FIELD AND PRESSURE DISTRIBUTION MEASUREMENTS ON BLUNT-NOSED BODIES AT M = 6.8. PARTS I AND II.

Part I describes the experimental measurement of sonic points between the bow shock waves and surfaces of three blunt-nosed bodies: a hemisphere, an ellipsoid and a hyperboloid. A comparison between these measurements and the theoretical sonic lines calculated by Mangler[1] shows reasonable agreement. Comparisons between the theoretical and the experimental bow shock wave shapes for these body configurations, together with their stand-off distances from the bodies shows very close agreement.

Pressure distribution measurements along the surfaces of the ellipsoid and hyperboloid are described in Part II. On the forward part of the bodies a comparison between the experimental pressure distribution and the theoretical pressure distribution calculated by Mangler shows good

(Over)

A.R.C. C.P. No.615. July, 1961
Osborne, W.K. and Crane, J.F.W.

FLOW FIELD AND PRESSURE DISTRIBUTION MEASUREMENTS ON BLUNT-NOSED BODIES AT M = 6.8. PARTS I AND II.

Part I describes the experimental measurement of sonic points between the bow shock waves and surfaces of three blunt-nosed bodies: a hemisphere, an ellipsoid and a hyperboloid. A comparison between these measurements and the theoretical sonic lines calculated by Mangler[1] shows reasonable agreement. Comparisons between the theoretical and the experimental bow shock wave shapes for these body configurations, together with their stand-off distances from the bodies shows very close agreement.

Pressure distribution measurements along the surfaces of the ellipsoid and hyperboloid are described in Part II. On the forward part of the bodies a comparison between the experimental pressure distribution and the theoretical pressure distribution calculated by Mangler shows good

(Over)

A.R.C. C.P. No.615. July, 1961
Osborne, W.K. and Crane, J.F.W.

FLOW FIELD AND PRESSURE DISTRIBUTION MEASUREMENTS ON BLUNT-NOSED BODIES AT M = 6.8. PARTS I AND II.

Part I describes the experimental measurement of sonic points between the bow shock waves and surfaces of three blunt-nosed bodies: a hemisphere, an ellipsoid and a hyperboloid. A comparison between these measurements and the theoretical sonic lines calculated by Mangler[1] shows reasonable agreement. Comparisons between the theoretical and the experimental bow shock wave shapes for these body configurations, together with their stand-off distances from the bodies shows very close agreement.

Pressure distribution measurements along the surfaces of the ellipsoid and hyperboloid are described in Part II. On the forward part of the bodies a comparison between the experimental pressure distribution and the theoretical pressure distribution calculated by Mangler shows good

(Over)

agreement. However, agreement becomes progressively worse downstream. The experimental pressure distributions compare fairly well with the modified Newtonian pressure distributions for the two bodies. The location of the sonic points on the surfaces of the bodies, deduced from the experimental pressure distribution, gives values which are compatible with the sonic point measurements in Part I.

agreement. However, agreement becomes progressively worse downstream.. The experimental pressure distributions compare fairly well with the modified Newtonian pressure distributions for the two bodies. The location of the sonic points on the surfaces of the bodies, deduced from the experimental pressure distribution, gives values which are compatible with the sonic point measurements in Part I.

agreement. However, agreement becomes progressively worse downstream. The experimental pressure distributions compare fairly well with the modified Newtonian pressure distributions for the two bodies. The location of the sonic points on the surfaces of the bodies, deduced from the experimental pressure distribution, gives values which are compatible with the sonic point measurements in Part I.

agreement. However, agreement becomes progressively worse downstream. The experimental pressure distributions compare fairly well with the modified Newtonian pressure distributions for the two bodies. The location of the sonic points on the surfaces of the bodies, deduced from the experimental pressure distribution, gives values which are compatible with the sonic point measurements in Part I.

Published by
HER MAJESTY'S STATIONERY OFFICE

To be purchased from
York House, Kingsway, London w.c.2
423 Oxford Street, London w.1
13A Castle Street, Edinburgh 2
109 St. Mary Street, Cardiff
39 King Street, Manchester 2
50 Fairfax Street, Bristol 1
35 Smallbrook, Ringway, Birmingham 5
80 Chichester Street, Belfast 1
or through any bookseller

Printed in England

S.O. CODE No. 23-9013-15